CrossMark

Microstructure and Thermoelectric Properties of Bulk Cobalt Antimonide (CoSb$_3$) Skutterudites Obtained by Pulse Plasma Sintering

M.J. KRUSZEWSKI [1,4] R. ZYBAŁA,[1] Ł. CIUPIŃSKI,[1] M. CHMIELEWSKI,[2]
B. ADAMCZYK-CIEŚLAK,[1] A. MICHALSKI,[1] M. RAJSKA,[3]
and K.J. KURZYDŁOWSKI[1]

1.—Faculty of Materials Science and Engineering, Warsaw University of Technology, Wołoska 141, 02-507 Warsaw, Poland. 2.—Institute of Electronic Materials Technology, Wólczyńska 133, 01-919 Warsaw, Poland. 3.—Faculty of Materials Science and Ceramics, AGH University of Science and Technology, Mickiewicza 30, 30-059 Krakow, Poland. 4.—e-mail: m.kruszewski@inmat.pw.edu.pl

The use of the pulse plasma sintering technique for CoSb$_3$ thermoelectric material consolidation is reported in this work. The influence of sintering temperature on the microstructure and material properties such as the Seebeck coefficient, electrical resistivity, and thermal conductivity has been investigated. It is shown that, for samples fabricated at 923 K and 973 K, there were no significant differences in the average grain size or final phase composition. In both cases, a fine-grained polycrystalline structure of the compacts with density nearly equal to the theoretical value was achieved. Both samples were composed almost uniquely of CoSb$_3$ phase. The measured thermoelectric parameters such as the Seebeck coefficient, electrical, and thermal conductivity showed similar dependence on temperature. For both samples, the Seebeck coefficient was negative at room temperature and showed a transition from n- to p-type conduction over the temperature range of 400 K to 460 K. The measured minimum thermal conductivity values, 4 W m^{-1} K^{-1} to 5 W m^{-1} K^{-1} at 723 K, are typical for undoped bulk CoSb$_3$. A maximum ZT value of 0.08 at 623 K was obtained for the sample consolidated at 923 K for 5 min. The results of this work are very promising from the point of view of use of pulse plasma sintering as an alternative method for fabrication of a broad range of thermoelectric materials in the future.

INTRODUCTION

Providing sustainable energy to the world's population is a major societal, technical, and scientific challenge of the 21st century, as fossil-fuel supplies decrease while world energy demands increase. Thermoelectric (TE) materials have potential applications in power generation devices that convert waste heat into electric current through the Seebeck effect, thus providing an alternative energy technology to reduce dependence on traditional, fossil fuels. The thermoelectric effect can also be used in solid-state Peltier coolers, which do not use environmentally harmful fluids. Thermoelectric devices also have the advantage of having no moving parts, making them silent, durable, and reliable.

The conversion efficiency of TE materials is determined by a dimensionless figure of merit defined as $ZT = \sigma S^2 T / \lambda$, where σ is the electrical conductivity, S is the Seebeck coefficient, T is the absolute temperature, and λ is the thermal conductivity. In general,

there are two ways to improve ZT and hence the conversion efficiency of a TE material. The first method is to increase the numerator, which is defined as the power factor (σS^2). The second is based on reduction of the thermal conductivity. However, obtaining high-ZT materials is a demanding challenge, because λ, S, and σ are interdependent. The thermal conductivity can be described as a sum of electric (λ_e) and lattice (λ_l) components. λ_e and σ are directly related through the Wiedemann–Franz law, $\lambda_e = L_0 \sigma T$, where L_0 is the Lorenz number. Therefore, the denominator should be minimized by an independent reduction of the lattice thermal conductivity λ_l, which is not determined by the electronic structure of the TE material.

One of the most promising material groups for mid-temperature applications is the skutterudites. These are compounds with general formula MX_3, where M is a metal such as Co, Rh, or Ir, and X is a pnictogen, such as P, Sb, or As.[1] Skutterudites crystallize with the structure of cobalt arsenide in regular space group $Im\text{-}3$. Their special features are the so-called cages in the crystal structure in which other atoms may be placed, thereby forming filled skutterudites. In recent years it has been shown that filling the cages with guest atoms provides an effective mechanism for reducing λ_l and also improves the power factor by modifying the electronic properties of the material.[2–4] Recent studies concerning indium filler have proven that In-filled $CoSb_3$ offers a unique combination of low λ_l together with high σ and large S.[5] Zhao et al. attributed this to the multilocalization transport behavior in the material, which is related to effective phonon scattering by In rattlers, accelerated electron movement due to charge transfer between Sb and In, and increase in the density of states near the Fermi level caused by enhanced hybridization of p–d orbitals between Co and Sb.

Currently, several methods are used to fabricate bulk $CoSb_3$. Typically, the process includes two stages: preparation of the alloy powder and its subsequent consolidation. The first stage may be achieved by methods such as solid-state reaction,[6,7] chemical alloying,[8,9] and mechanical alloying,[10] or by a solvothermal method.[11] In most cases, the second stage is achieved by a powder metallurgy technique such as hot pressing[6,9] or spark plasma sintering (SPS).[12–14] Recently, utilization of self-propagating high-temperature synthesis (SHS) as a very fast and effective method for skutterudite synthesis has been presented.[15] Those authors reported that $CoSb_{2.85}Te_{0.15}$ obtained by SHS with subsequent SPS exhibited a ZT value of 0.98 at 820 K, which is one of the highest ZT values presented in literature for unfilled $CoSb_3$-based thermoelectric material. Moreover, this fabrication route (SHS-SPS) has also proven effective for synthesis of other thermoelectric materials such as Bi_2Te_3, Mg_2Si, and Cu_2Se.[16]

In the present work, the use of the pulse plasma sintering (PPS) technique for consolidation of thermoelectric materials is reported. This method is a type of pulsed current method used in powder metallurgy, of which the most prominent representative is SPS. Both methods, i.e., PPS and SPS, use electric current as a direct source of heat, generated in the graphite punches, die, and sintered powder by the Joule effect. Despite the ongoing debate regarding whether plasma is induced during SPS consolidation,[17] both methods offer certain advantages over conventional sintering techniques (e.g., hot pressing), including:[18] (a) faster heating rate, (b) shorter annealing time, and (c) enhanced diffusion in the electric field. A comparison of the basic parameters of PPS and SPS is presented in Table I. PPS, schematically presented in Fig. 1a, is a very versatile method and has been successfully used in many applications including fabrication of metal-matrix[19,20] and ceramic-matrix[21] composites, welding of simple-[22] and complex-shaped element geometries,[23] as well as conducting ultrafast unconventional annealing of nanometals obtained by severe plastic deformation techniques.[24] In this work, a powder of the initial $CoSb_3$ alloy was prepared using a classic two-step process consisting of melting and long-term annealing, which is often used to synthesize homogeneously doped skutterudites (see, e.g., Ref. 25), for future use by the authors for synthesis of filled/doped $CoSb_3$-based thermoelectric materials. In this study, different sintering parameter values were used to determine the possible influence on the microstructure, phase composition, and thermoelectric properties of bulk $CoSb_3$ skutterudite material. The aim of this study is to compare the microstructure and thermoelectric properties of bulk $CoSb_3$ materials prepared via a combination of the classic two-step melting–annealing process and the PPS method.

EXPERIMENTAL PROCEDURES

Polycrystalline samples of $CoSb_3$ were prepared from metals of high purity. First, Co powder (99.98%, average particle size 2 μm) and Sb pieces (99.999%) were weighed according to stoichiometry with 2 at.% excess Sb, and loaded into a graphite-coated quartz ampoule. Then, the ampoule was sealed under vacuum ($\leq 5 \times 10^{-1}$ Pa) and placed in a rocking furnace for heat treatment. The sample was heated to 1173 K at 20 K/min and maintained at that temperature for 1 h, after which the power was switched off and the sample cooled down to room temperature in the furnace. Subsequently, the resulting material was ground using a hand mortar and again loaded into the quartz ampoule and sealed under vacuum. The second step of heat treatment was conducted at 923 K for 168 h. After this annealing, the resulting alloy was ground using a hand mortar and finally sintered in vacuum

Table I. Comparison of basic parameters of PPS and SPS[26,27]

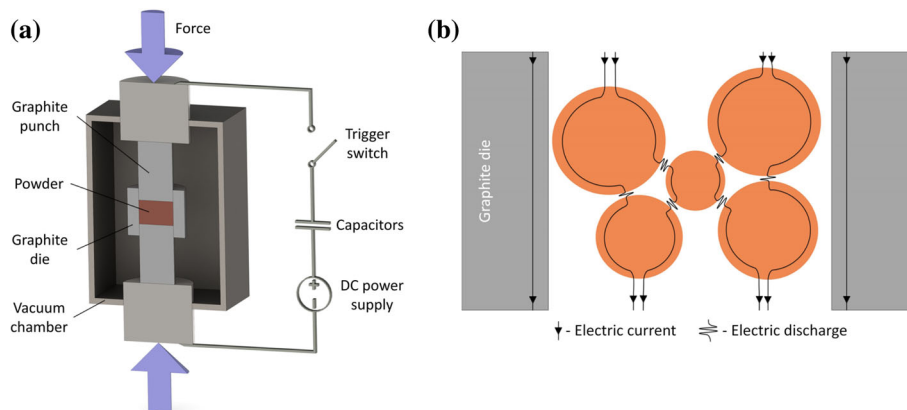| Parameter	Technique	
	PPS	**SPS (pulsed DC power supply)**
Pulse voltage	Up to 10,000 V	Usually up to 12 V
Pulse current	Up to 100 kA	Usually up to 10 kA
Pulse frequency	Up to 4 Hz	From Hz to kHz (depending on pulse pattern)
Pulse duration	150 ms to 250 ms (depending on the resistivity of the graphite die with powder)	From a few to tens of ms (depending on pulse pattern)

Fig. 1. (a) Schematic representation of the PPS technique; (b) pulsed electric current flow through a graphite die and powder particles during the initial step of the PPS process.

($\leq 10^{-3}$ Pa) under 60 MPa at 923 K to 973 K for 5 min using a pulse plasma sintering apparatus.

The density ρ of the samples with diameter and height of 10 mm was measured using the Archimedes method. Phase analysis was performed by x-ray diffraction (XRD, Bruker, D8 Advance, Cu K$_\alpha$). Powder morphology, fracture surfaces, microstructure, and chemical composition of the sintered samples were evaluated using scanning electron microscopy (SEM, Hitachi, SU-70) and energy-dispersive spectroscopy (EDS). The Seebeck coefficient, S, as well as the electrical conductivity, σ, were measured using the standard four-probe method in vacuum. The thermal diffusivity, α, was measured by the laser flash method (LFA, Netzsch, 457 MicroFlash) using samples with diameter of 10 mm and height of 1 mm. The thermal conductivity, λ, was calculated according to the formula $\lambda = \alpha \cdot C_p \cdot \rho$, where C_p is the theoretical heat capacity.[28] All measurements were performed over the temperature range of 323 K to 723 K.

RESULTS AND DISCUSSION

Figure 2 shows the XRD patterns of the CoSb₃ alloys after the first and second stage of heat treatment. The first heat treatment, conducted at 1173 K for 1 h followed by slow cooling, resulted in strong Bragg reflections of the CoSb₃ phase. How-

ever, some amount of unreacted Sb as well as CoSb₂ phase was detected. After the second step, conducted at 923 K for 168 h, apart from the CoSb₃ phase, a small amount of Sb remained in the alloy. The possible presence of a trace amount of Sb₂O₄ phase was also noted. The morphology of the ground skutterudite alloy after the first and second heat treatment is presented in Fig. 3a and b, respectively. Etching with concentrated nitric acid revealed that the final powder alloy was characterized by a grain size of 6 ± 3 μm. Its chemical composition obtained by EDS corresponds to a Co-to-Sb ratio of $1:3.07 \pm 0.03$, which is close to the initial stoichiometry. Subsequently, this powder was used for fabrication of bulk CoSb₃ samples.

Table II presents the PPS parameters used for consolidation of the bulk specimens. The sintering conditions were the same for both materials, except for the sintering temperature, which was higher for sample #2. The densities, which were approximately equal, indicated that almost full densification was achieved (the theoretical density of CoSb₃ being 7.621 g cm^{-3}[29]). This clearly demonstrates the advantage of PPS over conventional sintering techniques such as hot pressing, where full densification of CoSb₃ may be achieved only for higher temperatures and/or much longer annealing times.[30–32] The chemical composition was similar but not the same for the two samples. Sample #1,
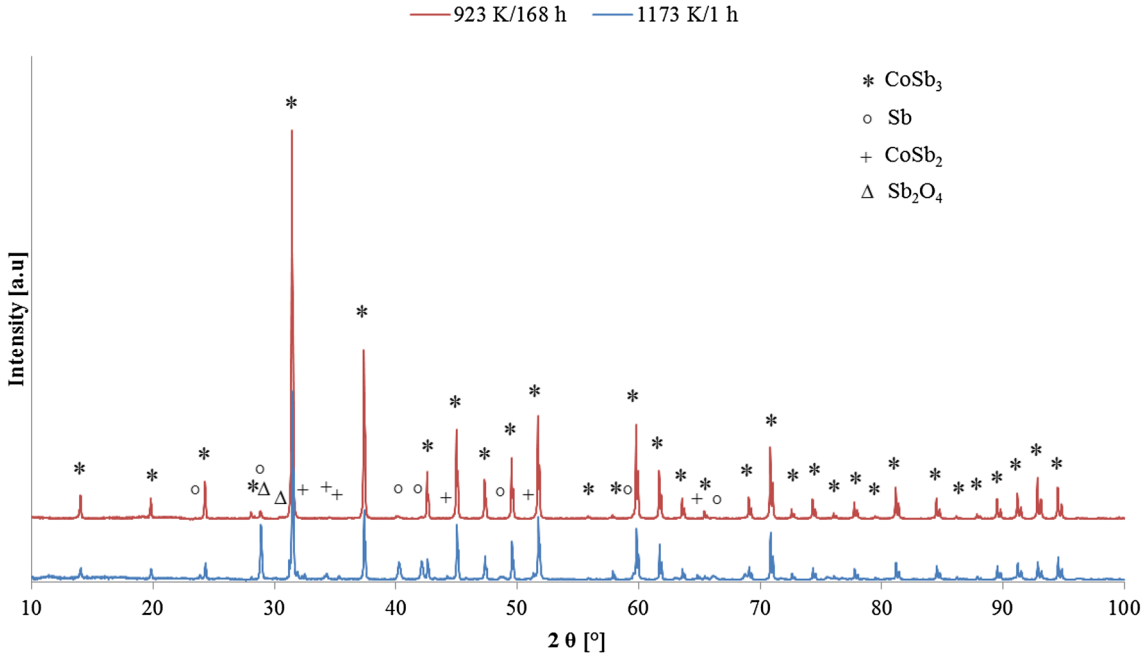
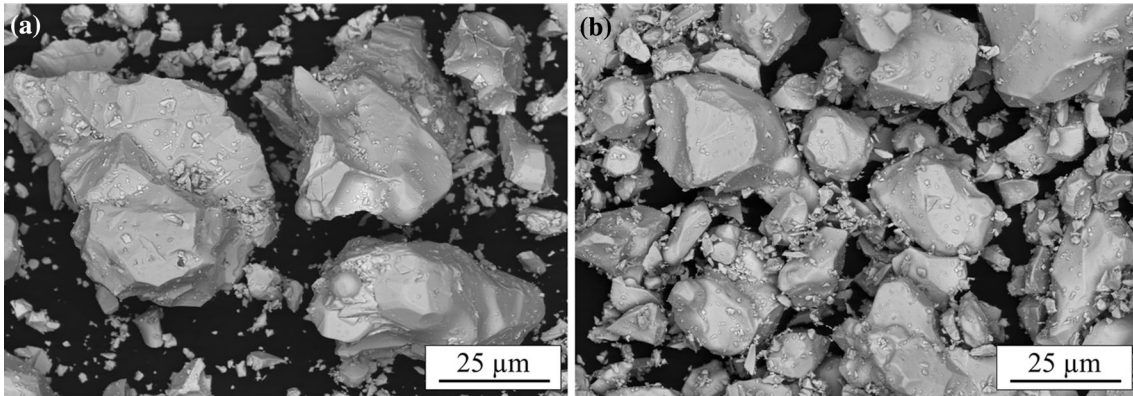Fig. 2. XRD patterns of CoSb$_3$ alloy after first and second heat treatment.

Fig. 3. SEM images of ground CoSb$_3$ alloy after first (a) and second (b) heat treatment.

Table II. PPS parameters and properties of fabricated CoSb$_3$ samples

Specimen	PPS conditions			Density (g cm^{-3})	Grain Size (μm)
	Pressure (MPa)	Temperature (K)	Time (min)		
#1	60	923	5	7.60	7 ± 6
#2	60	973	5	7.61	8 ± 6

which was fabricated at 923 K, had a Co-to-Sb ratio of 1:3.06 ± 0.02. The sample sintered at 973 K contained less Sb (1:3.04 ± 0.03). Accordingly, it may be stated that no evaporation of antimony was observed at 923 K but slight evaporation possibly occurred at 973 K.

Figure 4 presents the microstructure of the consolidated samples. Concentrated nitric acid was used for etching (Fig. 4a and c). It can be concluded that the PPS process conducted at 923 K and 973 K has a negligible effect on the sintered grain size (see Table II). Other studies (see, e.g., Refs. 32 and 33) showed that a grain size of 5 μm to 10 μm is stable at about 900 K even during annealing for a long time, and grain growth may be expected only during annealing at temperatures >1000 K. The fracture
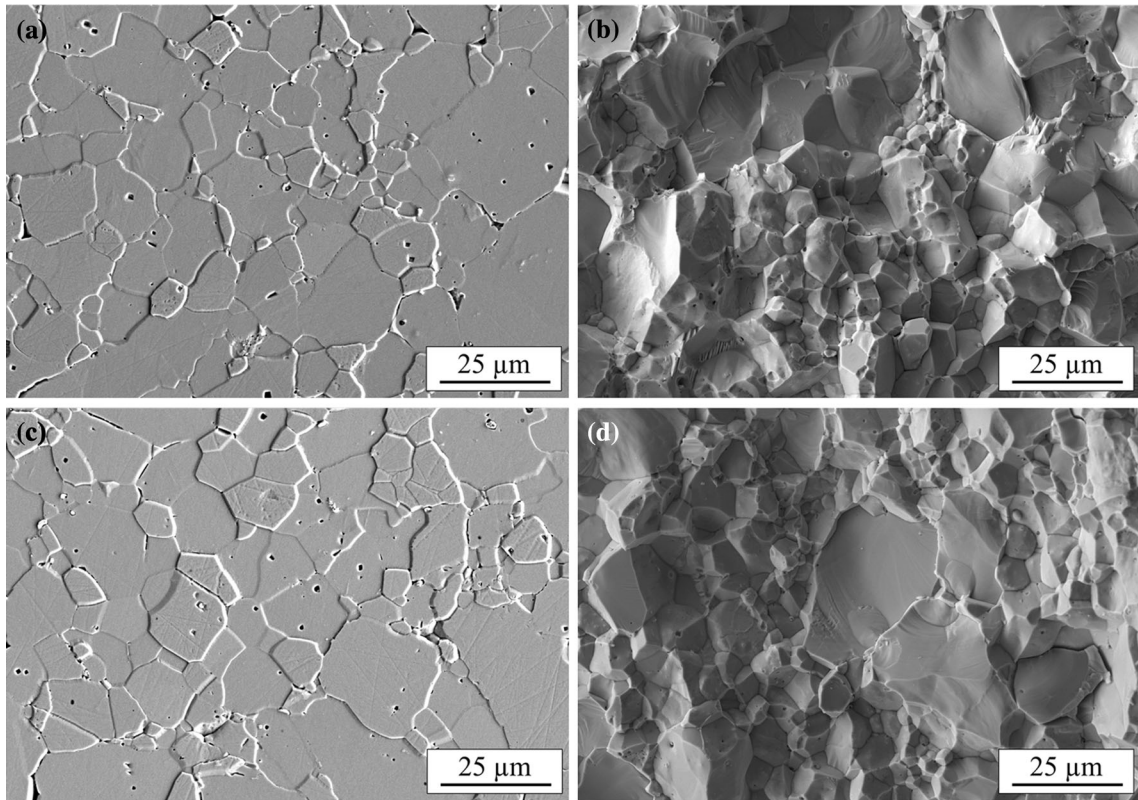
Microstructure and Thermoelectric Properties of Bulk Cobalt Antimonide (CoSb$_3$)
Skutterudites Obtained by Pulse Plasma Sintering

1373

Fig. 4. SEM images of microstructure and fracture surface of CoSb$_3$ samples fabricated at 923 K (a, b) and 973 K (c, d).
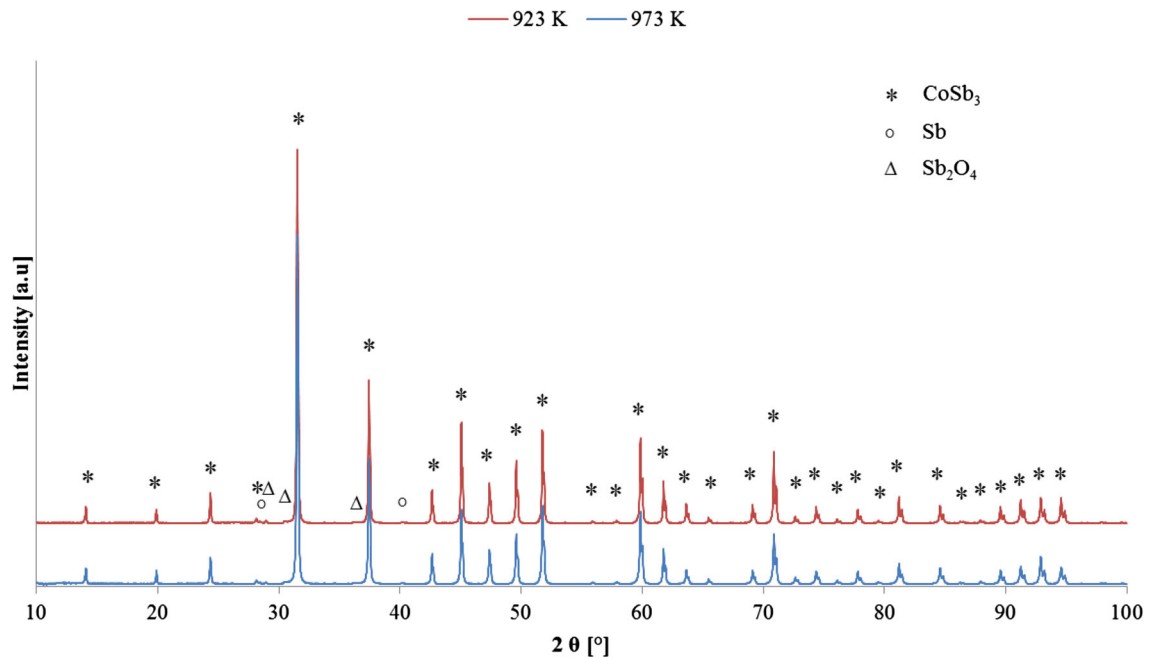

Fig. 5. XRD patterns of CoSb$_3$ samples consolidated at different temperatures.

surfaces of the two fabricated materials are presented in Fig. 4b and d.

Figure 5 shows the XRD patterns of the sintered CoSb$_3$ samples. The patterns are very similar to each other and correspond very well with the diffraction pattern obtained for the powder after the second step of the heat treatment process. The relatively short sintering time (5 min) has little effect
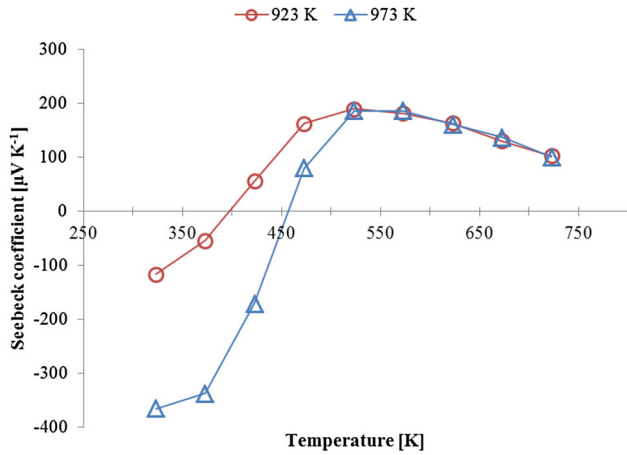
Fig. 6. Temperature dependence of Seebeck coefficient for $CoSb_3$ samples consolidated at different temperatures.

Fig. 7. Temperature dependence of electrical conductivity for $CoSb_3$ samples consolidated at different temperatures.

Fig. 8. Temperature dependence of calculated PF for $CoSb_3$ samples consolidated at different temperatures.

on the final phase compositions, which are dominated by $CoSb_3$.

Figure 6 presents the dependence of the Seebeck coefficient on temperature. At room temperature, both samples have negative Seebeck coefficient, indicating that electrons are the major charge carriers. However, with increasing temperature, the conduction changed from n- to p-type. This change occurs for sample #1 at around 400 K and for sample #2 at 460 K. This phenomenon is well known for the $CoSb_3$ skutterudite phase and was reported in previous studies, e.g., Refs. 12, 29, 34, and 35. The difference in the conduction-type transition temperature may be attributed to the different amount of excess Sb present in the samples. In Ref. [12] it was reported that this transition temperature shifted to lower values when the excess Sb in the samples increased from 0 at.% to 4 at.%, being about 550 K and 480 K, respectively. A larger surplus of Sb (6 at.% to 8 at.%) caused p-type conduction over the entire measurement temperature range. Comparing these results with those obtained in the present study, it can be noted that the transition temperature for both samples with 2 at.% excess Sb should occur at a higher temperature. A possible cause of this discrepancy may be attributed to the different fabrication route and its consequences. In Ref. [12] all samples were fabricated via mechanical alloying with subsequent SPS. High-energy ball milling conducted in a steel jar for 15 h may be responsible for introduction of iron impurities into the $CoSb_3$ alloy. As shown in Ref. [36], even a very small amount (0.1 at.%) of Fe may significantly change the temperature dependence of the Seebeck coefficient of $CoSb_3$. This effect, together with the reported volatilization of Sb,[12] may explain the higher conduction-type transition temperatures.

Figure 7 shows the temperature dependence of the electrical conductivity of the fabricated samples, being typical for semiconducting materials. At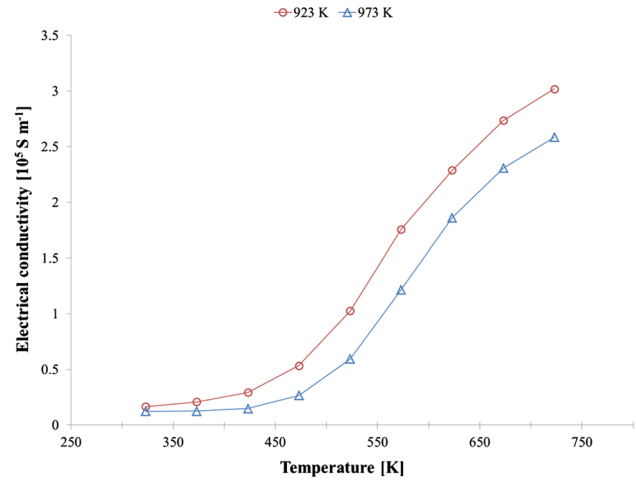 room temperature, both samples have virtually the same electrical conductivity, which increases with increasing temperature. A larger increase in electrical conductivity is observed for the sample fabricated at lower temperature.
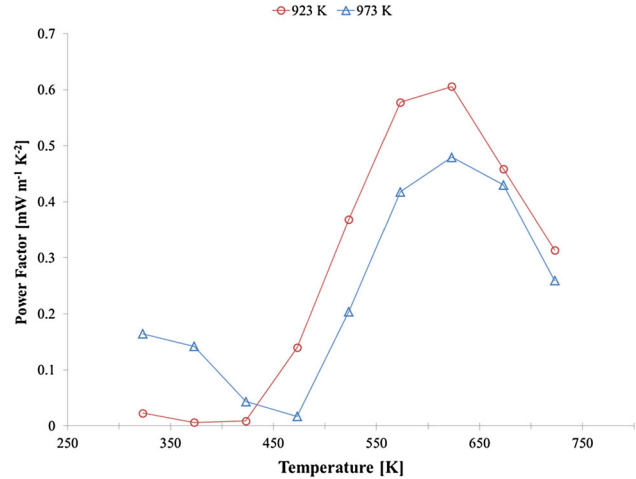
The calculated power factor (PF), presented in Fig. 8, shows two characteristic peaks, at low and high temperature. Such behavior is possible when the Seebeck coefficient changes sign. In this case, the smallest value of the power factor denotes the temperature at which the absolute value of the Seebeck coefficient reaches its minimum.

Figure 9 presents the temperature dependence of the thermal conductivity of the fabricated samples. The total thermal conductivity is the sum of the lattice contribution, λ_l, and the electronic component, λ_e. The latter parameter may be calculated using the Wiedemann–Franz law $\lambda_e = L_0 \sigma T$, where L_0 is the Lorenz number (2.45×10^{-8} W Ω K^{-2}). After subtraction of the calculated λ_e from the

Fig. 9. Temperature dependence of thermal conductivity for $CoSb_3$ samples consolidated at different temperatures. Dashed lines correspond to the lattice contribution to the overall thermal conductivity.
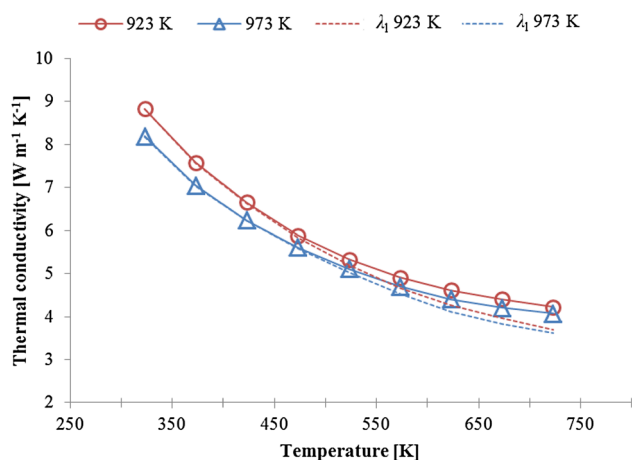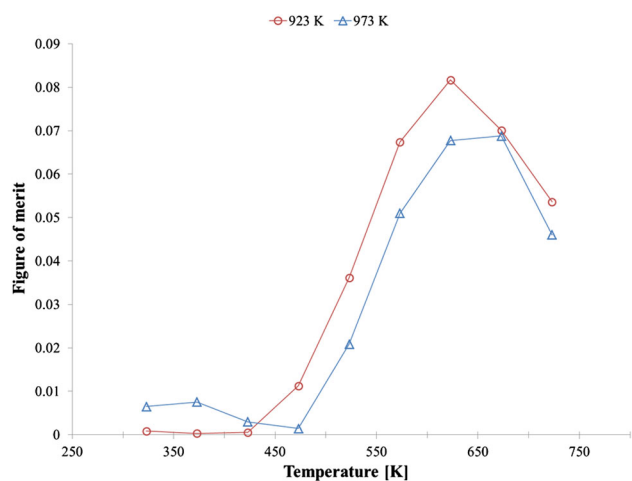

Fig. 10. Temperature dependence of ZT for $CoSb_3$ samples consolidated at different temperatures.

measured λ, the temperature dependence of the lattice contribution to the thermal conductivity may be plotted (dashed lines in Fig. 9). One can see that, for the fabricated polycrystalline $CoSb_3$ samples, the overall thermal conductivity is dominated by the lattice contribution, as is typical for undoped or lightly doped semiconductors.[29,37] The decrease in thermal conductivity with temperature is related to intensification of phonon scattering due to the Umklapp process, which is the dominant phonon scattering mechanism at high temperatures ($T \geq \theta_D$, where θ_D is the Debye temperature of 307 K[29] for $CoSb_3$).

Figure 10 shows the variation of the dimensionless figure of merit, ZT, with temperature, which corresponds very well with the PF shown in Fig. 8. The sample fabricated at 923 K has a maximum ZT of 0.08 at 623 K, while the sample fabricated at 973 K has a maximum ZT of 0.07 at 623 K to 673 K.

Current state-of-the-art $CoSb_3$-based skutterudite materials are characterized by $ZT > 1$, obtained by simultaneous modification of the chemical composition and microstructure.[38–40] The values of $ZT < 0.1$ presented in this work are similar to the results for pure $CoSb_3$ materials reported in literature.[12,41,42] Therefore, it can be concluded that the applied manufacturing process allowed production of high-quality, pure, undoped base material for use in further studies.

CONCLUSIONS

Bulk undoped $CoSb_3$ thermoelectric materials were successfully fabricated via a combination of the classic two-step melting–annealing process and the pulse plasma sintering method. Different sintering temperatures (923 K and 973 K) were used to evaluate the possible influence of the process parameters on the final microstructure, phase composition, and thermoelectric properties. Despite the difference in the sintering temperature, the materials possessed similar average grain size (7 μm to 8 μm) and phase composition. A small amount of Sb and a trace amount of Sb_2O_4 phase were detected after the final consolidation. For both samples, the Seebeck coefficient was negative at room temperature and showed a transition from n- to p-type conduction over the 400 K to 460 K temperature range. The difference between the transition temperatures was attributed to the different amount of excess Sb in the $CoSb_3$ alloy. It was shown that Sb volatilization might be minimized if the PPS process is conducted below 923 K for 5 min. The measured minimum thermal conductivity values (4 W m^{-1} K^{-1} to 5 W m^{-1} K^{-1} at 723 K) are typical for undoped bulk $CoSb_3$. A maximum ZT value of 0.08 at 623 K was obtained for the sample consolidated at 923 K for 5 min. The results of this work pave the way for use of pulse plasma sintering as an alternative method for fabrication of a broad range of thermoelectric materials in future studies.

REFERENCES

1. J.R. Sootsman, D.Y. Chung, and M.G. Kanatzidis, *Angew. Chem. Int. Ed. Engl.* 48, 8616 (2009).

2. J.R. Salvador, J. Yang, H. Wang, and X. Shi, *J. Appl. Phys.* 107, 043705 (2010).
3. X. Shi, J. Yang, J.R. Salvador, M. Chi, J.Y. Cho, H. Wang, S. Bai, J. Yang, W. Zhang, and L. Chen, *J. Am. Chem. Soc.* 133, 7837 (2011).
4. G.S. Nolas, X. Lin, J. Martin, M. Beekman, and H. Wang, *J. Electron. Mater.* 38, 1052 (2009).
5. W. Zhao, P. Wei, Q. Zhang, H. Peng, W. Zhu, D. Tang, J. Yu, H. Zhou, Z. Liu, X. Mu, D. He, J. Li, C. Wang, X. Tang, and J. Yang, *Nat. Commun.* 6, 6197 (2015).
6. L. Yang, J.S. Wu, and L.T. Zhang, *J. Alloys Compd.* 375, 114 (2004).
7. K.T. Wojciechowski, *J. Alloys Compd.* 439, 18 (2007).
8. A. Khan, M. Saleemi, M. Johnsson, L. Han, N.V. Nong, M. Muhammed, and M.S. Toprak, *J. Alloys Compd.* 612, 293 (2014).
9. Z. He, C. Stiewe, D. Platzek, G. Karpinski, E. Müller, S. Li, M. Toprak, and M. Muhammed, *J. Appl. Phys.* 101, 053713 (2007).
10. W.-S. Liu, B.-P. Zhang, J.-F. Li, and L.-D. Zhao, *J. Phys. D Appl. Phys.* 40, 566 (2007).
11. J.L. Mi, T.J. Zhu, X.B. Zhao, and J. Ma, *J. Appl. Phys.* 101, 054314 (2007).
12. W.-S. Liu, B.-P. Zhang, J.-F. Li, and L.-D. Zhao, *J. Phys. D Appl. Phys.* 40, 6784 (2007).
13. P. Nieroda, R. Zybala, and K.T. Wojciechowski, in *AIP Conference Proceedings* (2012), pp. 199–202.
14. R. Zybala and K.T. Wojciechowski, in *AIP Conference Proceedings* (2012), pp. 393–396.
15. T. Liang, X. Su, Y. Yan, G. Zheng, Q. Zhang, H. Chi, X. Tang, and C. Uher, *J. Mater. Chem. A* 2, 17914 (2014).
16. X. Su, F. Fu, Y. Yan, G. Zheng, T. Liang, Q. Zhang, X. Cheng, D. Yang, H. Chi, X. Tang, Q. Zhang, and C. Uher, *Nat. Commun.* 5, 4908 (2014).
17. J.G. Santanach, C. Estournès, A. Weibel, G. Chevallier, V. Bley, C. Laurent, and A. Peigney, *J. Eur. Ceram. Soc.* 31, 2247 (2011).
18. K. Sairam, J.K. Sonber, T.S.R.C. Murthy, C. Subramanian, R.K. Fotedar, P. Nanekar, and R.C. Hubli, *Int. J. Refract. Met. Hard Mater.* 42, 185 (2014).
19. A.M. Abyzov, M.J. Kruszewski, Ł. Ciupiński, M. Mazurkiewicz, A. Michalski, and K.J. Kurzydłowski, *Mater. Des.* 76, 97 (2015).
20. J. Grzonka, J. Kruszewski, M. Rosiński, Ł. Ciupiński, A. Michalski, and K.J. Kurzydłowski, *Mater. Charact.* 99, 188 (2015).
21. M. Rosiński, J. Wachowicz, T. Płociński, T. Truszkowski, and A. Michalski, *Ceram. Trans.* 243, 181 (2014).
22. M. Rosiński, M.J. Kruszewski, A. Michalski, E. Fortuna-Zaleśna, Ł. Ciupiński, and K.J. Kurzydłowski, *Fusion Eng. Des.* 86, 2573 (2011).
23. M.J. Kruszewski, Ł. Ciupiński, M. Rosiński, A. Michalski, and K.J. Kurzydłowski, *Fusion Eng. Des.* 88, 2573 (2013).
24. A.T. Krawczynska, T. Brynk, M. Rosinski, A. Michalski, S. Gierlotka, E. Grzanka, S. Stelmakh, B. Palosz, M. Lewandowska, and K.J. Kurzydlowski, in *Nanometals-Status Perspect. Proceedings of 33rd Risø International Symposium on Materials Science* (Roskilde, Denmark: Department of Wind Energy, Technical University of Denmark, 2012), p. 8.
25. X. Su, H. Li, G. Wang, H. Chi, X. Zhou, X. Tang, Q. Zhang, and C. Uher, *Chem. Mater.* 23, 2948 (2011).
26. G. Xie, O. Ohashi, K. Chiba, N. Yamaguchi, M. Song, K. Furuya, and T. Noda, *Mater. Sci. Eng. A* 359, 384 (2003).
27. U. Anselmi-Tamburini, J.E. Garay, and Z.A. Munir, *Mater. Sci. Eng. A* 407, 24 (2005).
28. Y. Cai, D. Zhao, X. Zhao, L. Chen, W. Jiang, and P. Zhai, *Mater. Trans.* 50, 782 (2009).
29. T. Caillat, A. Borshchevsky, and J.-P. Fleurial, *J. Appl. Phys.* 80, 4442 (1996).
30. M.-J. Kim and I.-H. Kim, *Met. Mater. Int.* 16, 459 (2010).
31. L. Yang, J.S. Wu, and L.T. Zhang, *Mater. Des.* 25, 97 (2004).
32. H. Nakagawa, H. Tanaka, A. Kasama, H. Anno, and K. Matsubara, in *XVI ICT"97. Proc. ICT"97. 16th International Conference on Thermoelectrics (Cat. No. 97TH8291)* (IEEE, 1997), pp. 351–355.
33. K.T. Wojciechowski, J. Toboła, and J. Leszczynski, *J. Alloys Compd.* 361, 19 (2003).
34. M.S. Toprak, C. Stiewe, D. Platzek, S. Williams, L. Bertini, E. Müller, C. Gatti, Y. Zhang, M. Rowe, and M. Muhammed, *Adv. Funct. Mater.* 14, 1189 (2004).
35. J.X. Zhang, Q.M. Lu, K.G. Liu, L. Zhang, and M.L. Zhou, *Mater. Lett.* 58, 1981 (2004).
36. S. Katsuyama, Y. Shichijo, M. Ito, K. Majima, and H. Nagai, *J. Appl. Phys.* 84, 6708 (1998).
37. K. Wojciechowski, P. Nieroda, J. Toboła, and R. Zybała, *Ceram. Mater.* 62, 60 (2010).
38. T. Dahal, Q. Jie, W. Liu, K. Dahal, C. Guo, Y. Lan, and Z. Ren, *J. Alloys Compd.* 623, 104 (2015).
39. G. Rogl, A. Grytsiv, P. Rogl, E. Bauer, M. Kerber, M. Zehetbauer, and S. Puchegger, *Intermetallics* 18, 2435 (2010).
40. G. Rogl, A. Grytsiv, P. Rogl, E. Royanian, E. Bauer, J. Horky, D. Setman, E. Schafler, and M. Zehetbauer, *Acta Mater.* 61, 6778 (2013).
41. C. Soon-Mok, L. Jae-Ki, S. Won-Seon, L. Hong-Lim, and K. Il-Ho, *J. Korean Phys. Soc.* 57, 1010 (2010).
42. W.-S. Liu, B.-P. Zhang, J.-F. Li, H.-L. Zhang, and L.-D. Zhao, *J. Appl. Phys.* 102, 103717 (2007).